High-Performance Bilayer Sliding $PtSe_2$ Infrared Photodetector

Zhihao Qu(屈志豪)[1], Yuhang Zhang(张宇航)[1], XinWei Zhao(赵辛未)[2], Yinan Wang(王义楠)[1], Fang Yang(杨昉)[1*], Weiwei Zhao(赵伟玮)[1*], and HongWei Liu(刘宏微)[1*]

[1]*Jiangsu Key Lab on Opto-Electronic Technology, School of Physics and Technology, Nanjing Normal University, Nanjing 210023, China*
[2]*School of Physics, Southeast University, Nanjing 211189, China*

(Received 15 January 2025; accepted manuscript online 27 March 2025)

The weak interlayer van der Waals (vdW) interactions in two-dimensional (2D) vdW materials enable sliding ferroelectricity as an effective strategy for modulating their intrinsic properties. In this work, we systematically investigate the influence of interlayer sliding on the electronic behavior of $PtSe_2$ using density functional theory (DFT) calculations. Our results demonstrate that interlayer sliding induces a pronounced photocurrent spanning the short-wavelength infrared to visible spectral ranges. Remarkably, under an applied gate voltage, the sliding ferroelectric $PtSe_2$ exhibits anomalously enhanced photovoltaic performance and an ultrahigh extinction ratio. Transmission spectral analysis reveals that this phenomenon originates from band structure modifications driven by energy-level transitions. Furthermore, the observed photocurrent enhancement via sliding ferroelectricity demonstrates universality across diverse platinum-based optoelectronic devices. This study introduces a novel paradigm for tailoring the intrinsic characteristics of 2D vdW semiconductors, expanding the design space for next-generation ferroelectric materials in advanced optoelectronic applications.

DOI: 10.1088/0256-307X/42/5/058101 CSTR: 32039.14.0256-307X.42.5.058101

Two-dimensional van der Waals (vdW) layered ferroelectric semiconductors demonstrate a distinctive integration of electrically switchable ferroelectric polarization and intrinsic electronic band structure properties.[1–3] These advancements enable the realization of substantial physical and technological potentials in nanoelectronics, with applications spanning diverse domains including neuromorphic computing architectures and high-efficiency photovoltaic energy conversion systems.[4–10] However, the limited availability of two-dimensional layered crystals categorized in noncentrosymmetric polar space groups has presented a fundamental obstacle to advancing research on intrinsic ferroelectricity in low-dimensional material systems. To date, only a few have been experimentally verified, including $CuInP_2S_6$, In_2Se_3, and MX compounds.[11,12]

Current research efforts are predominantly concentrated on the exploration of emerging two-dimensional ferroelectric semiconductors. The inherent weak interlayer vdW interactions in these layered materials have enabled the realization of interlayer sliding ferroelectricity through precise structural modification strategies, particularly via interlayer twisting engineering in moiré superlattice configurations and transition metal dichalcogenide (TMD)-based heterostructures.[7,13–15] Recently, a promising avenue has opened up for multiple 2D materials: inducing vertical polarization in their bilayer and multilayer configurations by stacking the layers in an interlayer inequivalent manner.[16–19] This polarization state, which exhibits reversible switching through interlayer sliding, demonstrates electrically tunable characteristics via external field manipulation. Notably, this emerging physical phenomenon has been experimentally verified in multiple vdW structures, including bilayer configurations and vertically stacked multilayer systems, as evidenced by recent advancements in the field, encompassing BN, InSe, and numerous TMDs (e.g., MoS_2, WSe_2, WTe_2, $PtTe_2$).[20–27] Researchers are also very interested in using 2D materials to apply sliding ferroelectricity to photovoltaic applications, such as Yang *et al.* developed an efficient photovoltaic device using slipped MoS_2,[28] achieving a photocurrent two orders of magnitude higher than 2H-MoS_2 by leveraging the depolarization field. Wu *et al.* found that bilayer and four-layer slipped MoS_2 structures exhibited rapid directional carrier transfer driven by a polarization field, resulting in a spontaneous photovoltaic effect.[29] Additionally, Yasuda demonstrated a non-volatile memory based on slipped BN,[30] where a gate electric field as low as 0.2 V/nm enhanced polarization charge rearrangement, significantly improving carrier mobility. However, there are still few reports on polarization-sensitive photodetection driven by interlayer sliding and gated regulation in the infrared range.

In this Letter, we employed first-principles calculations to investigate the behavior of 1T-$PtSe_2$ under interlayer sliding. Our findings reveal that sliding induces a polarization-sensitive self-powered photodetector, and its photocurrent enhancement ratio can be further enhanced

*Corresponding author. Email: 06299@njnu.edu.cn; jianpiao1986@163.com; 06254@njnu.edu.cn
© 2025 Chinese Physical Society and IOP Publishing Ltd. All rights, including for text and data mining, AI training, and similar technologies, are reserved.

through gating. These results offer significant theoretical insights that will guide the future design of photovoltaic ferroelectrics.

As depicted in Fig. 1(a), we have constructed models of pristine $PtSe_2$ alongside two interlayer sliding $PtSe_2$ models.[31–33] Previous research has established the 1T stacking of $PtSe_2$ as the prevalent and stable stacking pattern, serving as the pristine structure. Upon sliding, the symmetry shifts from D_{3d} to C_{3v}, resulting in the breaking of spatial inversion symmetry. The absence of imaginary frequencies in the phonon dispersion spectra verifies the thermodynamic stability of the sliding configuration, as illustrated in Fig. S1. Meanwhile, the discussion of the results of interface formation energy in supplementary material also indicates that the slip phase can exist stably in nature. Afterward, we employed the nudged elastic band (NEB) method[34] to model the migration kinetics process from α-$PtSe_2$ to β-$PtSe_2$ as shown black line in Fig. 1(b). Importantly, the energy barrier between the two polarized phases is only 30.1 meV, which is considerably lower than that of α-In_2Se_3 (50 meV) and $PtTe_2$ (56 meV).[12,24] Moreover, the red line in Fig. 1(b) represents the ferroelectric switching of the slip-stacked $PtSe_2$ along the reaction path, the vertical polarization value is 1.28 pc/m, and polarization intensity at the interface exhibits centrosymmetry along the migration path, indicating the reversal of out-of-plane ferroelectricity. Additionally, the difference in electrostatic potential energy for the structures driven by the polarization field is shown in Fig. S2, and we compared the absorption spectra and dielectric functions of the pristine structure and the slipping and stacking $PtSe_2$ (Fig. S3). As shown in Fig. 1(c) and Fig. S4, the original structure's differential charge density displays a symmetric distribution. However, the polarized phase, formed by rotation and sliding, demonstrates an asymmetric charge distribution. This observation implies that the sliding variation results in the different polarization direction in both interlayer sliding $PtSe_2$ layers, denoted as $+P$ and $-P$ in Fig. 1(a). The conduction band minimum (CBM) and valence band maximum (VBM) of the band gaps in these two phases originate from distinct layers, and the conditions are reversed between the two phases. Figure 1(d) and Fig. S5 illustrate the band alignment for both α-$PtSe_2$ and β-$PtSe_2$, revealing a type-II band alignment. This alignment indicates that the natural electric field present in sliding $PtSe_2$ promotes the movement of electrons and holes to separate layers, and interlayer sliding can be equivalent to the translation of rigid ions without vertical displacement, thus the origin of vertical polarization is purely electronic.[17] To further investigate the evolution of the electronic properties of the sliding structures, we also calculated the electronic properties of monolayer $PtSe_2$ and pristine $PtSe_2$, as shown in Fig. S6. We employed the PBE method to calculate their band structures. The bandgap of monolayer $PtSe_2$ is 1.29 eV, while the bandgap of bilayer $PtSe_2$ is 0.15 eV, which is consistent with the results reported in other literature. The bandgap of $PtSe_2$ decreases rapidly as the number of layers increases. Notably, the bandgap of the sliding structure is 0.45 eV, which is larger than that of the pristine structure. This increase in bandgap is attributed to the inhomogeneous distribution of interfacial electrons caused by the sliding, which enhances the repulsive van der Waals interactions between the layers and increases the interlayer distance (from 2.26 Å to 2.66 Å), thereby leading to an increase in the band gap.

To further study the theoretical performance of ferroelectric photovoltaic devices, we crafted photodetector models encompassing the pristine $PtSe_2$, α-$PtSe_2$, and β-$PtSe_2$ as illustrated in Fig. 2(a) and Fig. S7, comprehensive details included in the SI. Additionally, we utilized the Nanodcal[35] software package to investigate the photoelectric response (0.8–3.2 eV) generated by the photogalvanic effect (PGE),[36,37] which is a software based on density functional theory within the nonequilibrium Green's function method (NEGF). Figure 2(b) depicts the response photocurrents of the three device structures when exposed

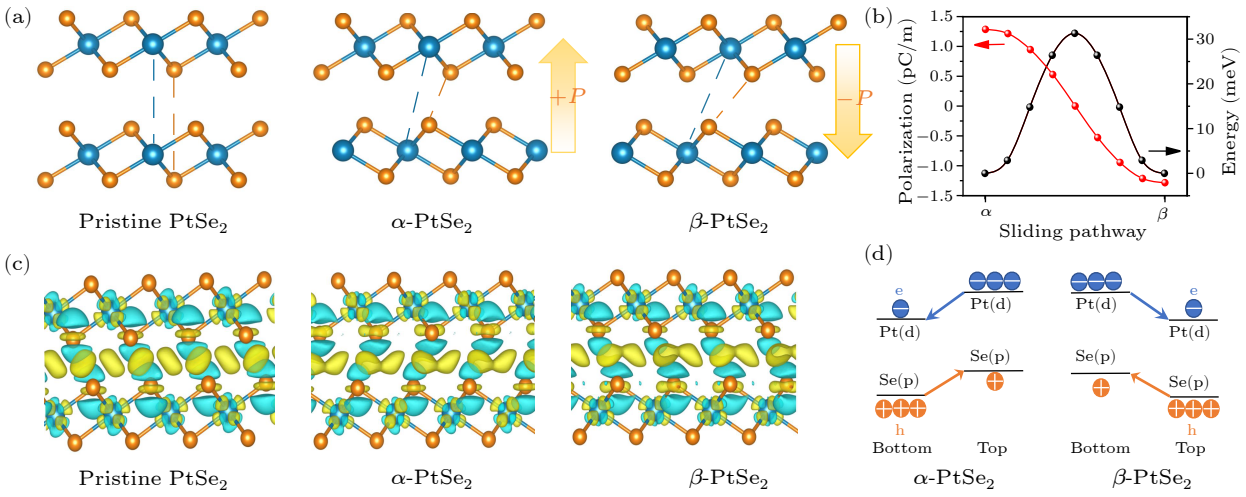

Fig. 1. Depicts the schematic and properties of the sliding $PtSe_2$. (a) Structural illustrations of the pristine $PtSe_2$ and the sliding structures. (b) The black line represents the migration barrier, and the red line is the polarization value of the structure corresponding to the polarization path. (c) Partial charge densities of the original $PtSe_2$ and the polarized phases. (d) Schematic illustrations of band alignments for the upper-polarized and lower-polarized phases, respectively.

to linearly polarized light with varying angles without bias. Combined with the previous discussion on the out-of-plane polarization, this is consistent with the theoretical phenomenon of the nonsynchronous bulk photovoltaic effect proposed by Xiao,[38] interlayer sliding $PtSe_2$ generates a non-switchable in-plane photo-induced photocurrent and a switchable out-of-plane carrier flows. The photocurrent varies as a function of polarization angle for the three devices under zero bias conditions, as depicted in Fig. 2(b) and Fig. S8, further confirming the anisotropic carrier mobility in the $PtSe_2$. Interestingly, the intensities of photoresponses in α-$PtSe_2$ and β-$PtSe_2$ are significantly higher, by order of magnitude, when a local gate voltage of 1 V is applied to the central region of the so-called model scattering area, compared to those without the gate voltage, as shown in Fig. 2(c). In the pristine device, a feeble photocurrent is observed that the peak value does not exceed 0.34, and the application of a gate voltage does not significantly boost the photocurrent. Contrastingly, the introduction of gate voltage to both α-$PtSe_2$ and β-$PtSe_2$ devices leads to a remarkable amplification of photocurrent across all photon energy ranges with most peak photocurrents surpassing 0.1. This enhancement is particularly pronounced in the 1.6–3.2 eV range, where multiple response peaks are observed. For instance, α-$PtSe_2$ shows peak photocurrents of 1.12, 1.19, and 0.75 at 2.3 eV, 2.4 eV, and 2.8 eV respectively, which significantly exceed the corresponding values without a gate voltage: 0.16, 0.07, and 0.07. Similarly, β-$PtSe_2$ experiences peak photocurrents of 1.28 (compared to 0.03 without a gate voltage), 1.17 (0.01), and 1.06 (0.81) at 2.4 eV, 2.6 eV, and 3.2 eV respectively, as shown in Figs. 2(c3)–2(c6).

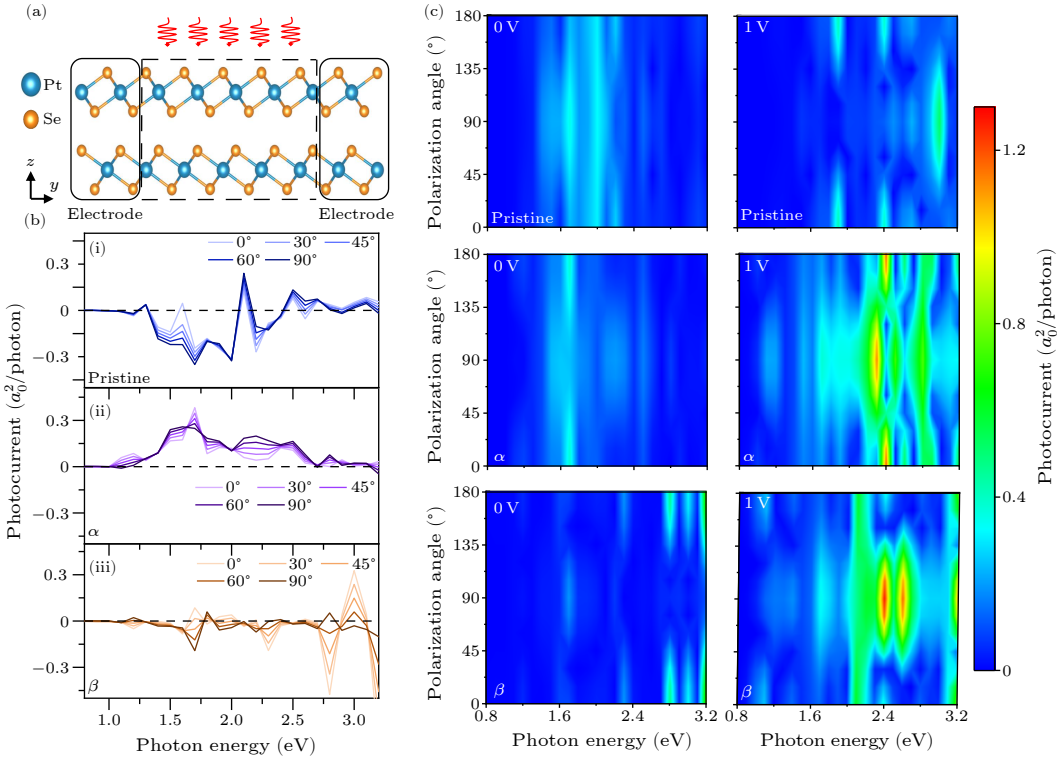

Fig. 2. (a) Schematic diagram of a two-electrode device under illumination by linearly polarized light for structure α-$PtSe_2$. (b) The photocurrent of the three structures under illumination by linearly polarized light with varying polarization angles, and (c) The photocurrent of the three structures, both without and with the application of a gate voltage. The left side depicts the photocurrent without a gate voltage, while the right side represents the photocurrent with a gate voltage applied.

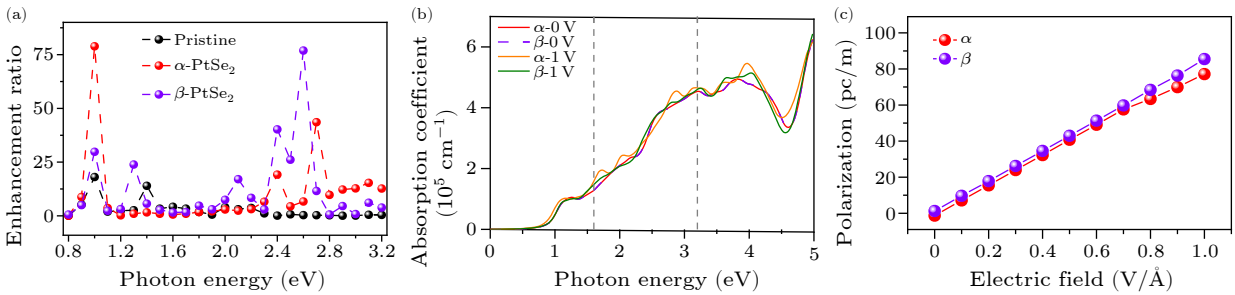

Fig. 3. (a) The photocurrent enhancement ratio of pristine $PtSe_2$, α-$PtSe_2$ and β-$PtSe_2$ after the application of a gate voltage compared to their performance without a gate voltage. (b) Comparison of the absorption spectra of A and B before and after applying a gate voltage of 1 V, and (c) The variation of polarization strength under different structures concerning the external vertical electric field.

Furthermore, we have compared the photocurrent enhancement ratios of gated and ungated structures, shown in Fig. 3(a). The highest enhancement ratios for the two polarization phases were observed at 2.6 eV and 1.0 eV, reaching 76.9 and 78.8, respectively. To further analyze the cause, we have calculated the transmission spectra, as illustrated in Fig. S9.

To analyze the cause, we calculated the polarization values and absorption spectra of α-$PtSe_2$ and β-$PtSe_2$ under the 1 V vertical electric field. The results show that under the action of an external electric field, the polarization values of the two structures in the out-of-plane direction are significantly and approximately linearly enhanced. Under 1 V external electric field, the polarization values are 77.15 pc/m and 85.51 pc/m, respectively. Additionally, the absorption spectra indicate that the absorption coefficients of α-$PtSe_2$ and β-$PtSe_2$ under electric field exhibit only a slight enhancement under an external electric field within the visible to infrared range. Therefore, we speculate that the positive coupling between the applied gate voltage and the out-of-plane polarization of interlayer slipping greatly promotes the depolarization field of the slipped structure, ultimately enhancing the separation and transport of photogenerated carriers. In addition, to further investigate the impact of broken spatial inversion symmetry on the device, we introduced the Asymmetry factor as a parameter to quantitatively characterize the structural asymmetry, as illustrated in Fig. S10. It is clearly observable that Asymmetry factor exhibits a significant increase following the application of the gate voltage. This bears a resemblance to the conclusions drawn by Lian.[39] Moreover, its growth trend qualitatively aligns with the variation trend of the photocurrent enhancement ratio, which further substantiates that the enhancement of the photoresponse current is primarily due to the asymmetric spatial distribution of charges in the device structure, which disrupts the spatial inversion symmetry of the structure.

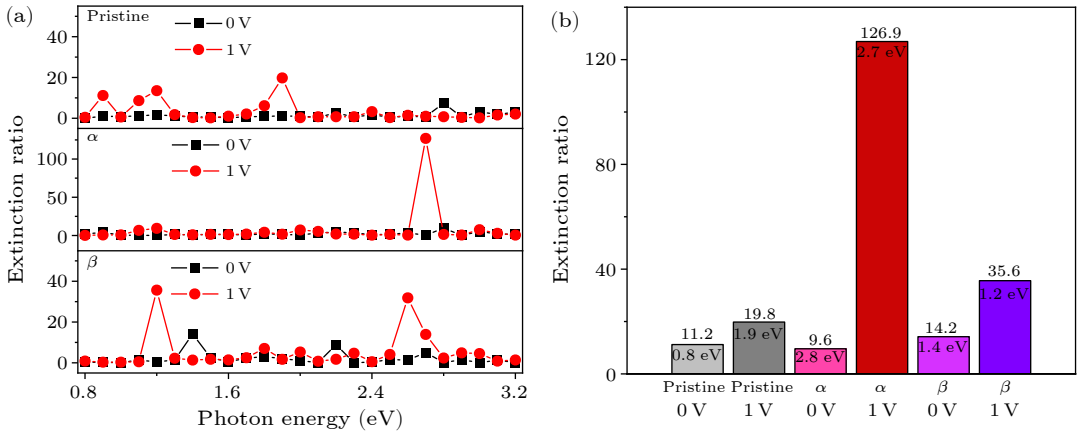

Fig. 4. (a) The extinction ratios of pristine $PtSe_2$, α-$PtSe_2$, and β-$PtSe_2$ under varying photon energies, both with and without the application of a gate voltage. (b) The corresponding maximum extinction ratios for each structure in different conditions.

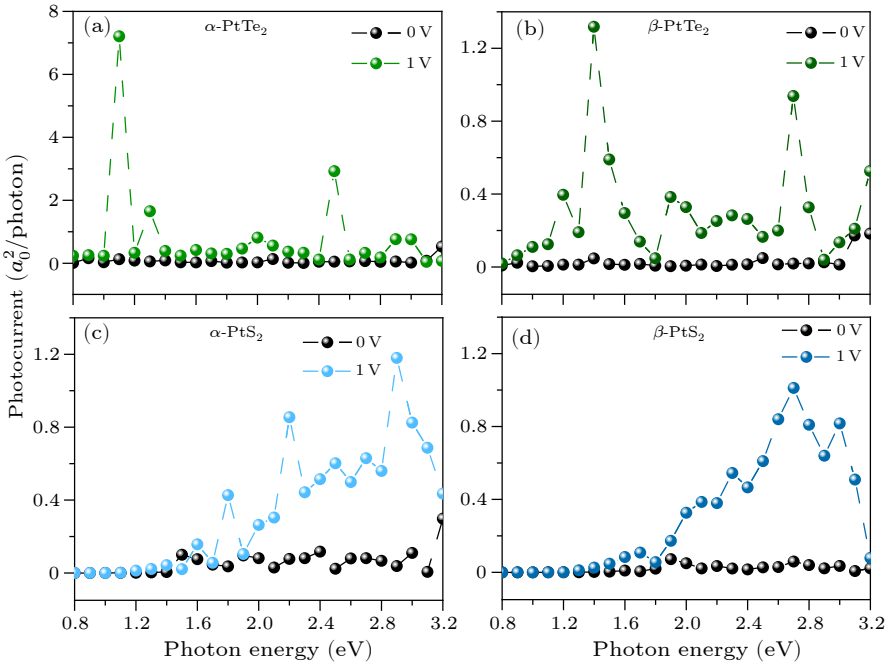

Fig. 5. The PGE photocurrents of $PtTe_2$ and PtS_2 sliding devices are represented by (a)–(d), respectively.

Figure 4(a) showcases the extinction ratio variation of the three distinct structures. Notably, while the pristine $PtSe_2$ shows a small increase in its extinction ratio with the application of a gate voltage, α-$PtSe_2$ and β-$PtSe_2$ display a significant boost. Figure 4(b) compares the peak extinction ratios attained both with and without the application of a gate voltage. In the absence of a gate voltage, the maximum extinction ratios for pristine $PtSe_2$, α-$PtSe_2$, and β-$PtSe_2$ are 11.2, 9.6, and 14.2, respectively. With the introduction of a gate voltage, these peak extinction ratios experience substantial growth, soaring to 19.8, 126.9, and 35.6 at photon energies of 1.9 eV, 2.7 eV, and 1.2 eV, respectively. This underscores the high polarization sensitivity exhibited by sliding $PtSe_2$ optoelectronic devices when controlled by a gate voltage, making them exceptionally suitable for polarization detection.

The photocurrents for $PtTe_2$ and PtS_2 after sliding were also calculated, as shown in Figs. 5(a)–5(d). Notably, the application of a gate voltage also boosted the photocurrent in each structure. Specifically, the peak photocurrents for gate applied α-$PtTe_2$ and β-$PtTe_2$ reached 7.21 and 1.32, respectively, corresponding to photon energies of 1.1 eV and 1.4 eV. Likewise, the peak photocurrents observed in α-PtS_2 and β-PtS_2 were 1.18 (2.9 eV) and 1.01 (2.7 eV), respectively. We also explored the asymmetry factor for $PtTe_2$ and PtS_2. It can be observed that the A values for both $PtTe_2$ and PtS_2 exhibit a significant increase after the application of the gate voltage, as shown in Fig. S11. This also indicates that the enhancement of the photoresponse current is primarily due to the asymmetric spatial distribution of charges in the structure, which disrupts the spatial inversion symmetry of the structure. This indicates that interlayer slid PtX_2 (X = S, Se, Te) materials exhibit the universal potential for light detection applications, spanning the near-infrared to visible spectrum.

In summary, we have successfully designed two ferroelectric phases of $PtSe_2$, achieved through interlayer sliding. This sliding disrupts the original high-symmetry spatial configuration, thereby generating PGE photocurrent. By applying an out-of-plane gate voltage, we disrupt the carrier distribution symmetry of the structure. This results in a remarkable photocurrent enhancement, accompanied by an exceptionally high extinction ratio. Our theoretical investigation offers a strategy to significantly amplify the PGE photocurrent and provides valuable insights for creating switchable photoelectric devices.

See the supplementary material for (i) the details of the calculations about atomic structures and devices; (ii) the phonon spectrum and electronic properties of α-$PtSe_2$ and β-$PtSe_2$; (iii) device models of primitive structure and β–$PtSe_2$; (iv) Polarized photocurrent and photoelectric properties of devices under different gate voltages.

Acknowledgements. This work was supported by the National Key Research and Development Program of China (Grant No. 2024YFB3211701), the National Natural Science Foundation of China (Grant Nos. T2222011, 62174026, and 12274234), the National Key Research and Development Program of China (Grant Nos. 2023YFB3611400 and 2019YFA0308000), and the Fundamental Research Funds for the Central Universities (Grant No. 242023k30027). The computational resource was supported by Hongzhiwei Technology.

References

[1] Valasek J 1921 *Phys. Rev.* **17** 475
[2] Wang Z, Gui Z G, and Huang L 2023 *Phys. Rev. B* **107** 035426
[3] Jiang X X, Wang Z K, Li C, Sun X L, Yang L, Li D M, Cui B, and Liu D S 2024 *Chin. Phys. Lett.* **41** 057501
[4] Meng P, Wu Y Z, Bian R J, Pan E, Dong B, Zhao X X, Chen J G, Wu L S, Sun Y Q, Fu Q D, Liu Q, Shi D, Zhang Q, Zhang Y W, Liu Z, and Liu F C 2022 *Nat. Commun.* **13** 7696
[5] Wang X R, Yasuda K, Zhang Y, Liu S, Watanabe K, Taniguchi T, Hone J, Fu L, and Jarillo-Herrero P 2022 *Nat. Nanotechnol.* **17** 367
[6] Wang Q, Liang Y, Yao H, Li J W, Liu T W, Frauenheim T, Wang B, and Wang J 2022 *J. Mater. Chem. C* **10** 1048
[7] Li L and Wu M 2017 *ACS Nano* **11** 6382
[8] Lin Z Z, Si C, Duan S R, Wang C, and Duan W H 2019 *Phys. Rev. B* **100** 155408
[9] Wei C J, Jiazila N, Liu X Y, Song P, Gao H, Sun J Q, Bao L H, Lin X, and Gao H J 2024 *Chin. Phys. Lett.* **41** 128501
[10] Zhao Y H, Liu B, Yang J L, He J, and Jiang J 2020 *Chin. Phys. Lett.* **37** 088501
[11] Liu F C, You L, Seyler K L, Li X B, Yu P, Lin J H, Wang X W, Zhou J D, Wang H, He H Y, Pantelides S T, Zhou W, Sharma P, Xu X D, Ajayan P M, Wang J L, and Liu Z 2016 *Nat. Commun.* **7** 12357
[12] Zhou Y, Wu D, Zhu Y H, Cho Y, He Q, Yang X, Herrera K, Chu Z D, Han Y, Downer M C, Peng H L, and Lai K J 2017 *Nano. Lett.* **17** 5508
[13] Rogée L, Wang L J, Zhang Y, Cai S H, Wang P, Chhowalla M, Ji W, and Lau S P 2022 *Science* **376** 973
[14] van Wijk M M, Schuring A, Katsnelson M I, and Fasolino A 2014 *Rev. Lett.* **113** 135504
[15] Ding N, Chen J, Gui C R, You H P, Yao X Y, and Dong S 2021 *Phys. Rev. Materials* **5** 084405
[16] Miao L P, Ding N, Wang N, Shi C, Ye H Y, Li L, Yao Y F, Dong S, and Zhang Y 2022 *Nat. Mater.* **21** 1158
[17] Yang L, Ding S P, Gao J H, and Wu M H 2023 *Phys. Rev. Lett.* **131** 096801
[18] Yang L and Wu M 2023 *Adv. Funct. Mater.* **33** 2301105
[19] Fei Z Y, Zhao W J, Palomaki T A, Sun B S, Miller M K, Zhao Z Y, Yan J Q, Xu X D, and Cobden D H 2018 *Nature* **560** 336
[20] Shi J, Yu P, Liu F C, He P, Wang R, Qin L, Zhou J B, Li X, Zhou J D, Sui X Y, Zhang S, Zhang Y F, Zhang Q, Sum T C, Qiu X H, Liu Z, and Liu X F 2017 *Adv. Mater.* **29** 1701486
[21] Dong Y, Yang M M, Yoshii M, Matsuoka S, Kitamura S, Hasegawa T, Ogawa N, Morimoto T, Ideue T, and Iwasa Y 2023 *Nat. Nanotechnol.* **18** 36
[22] Wang Q S, Zheng J C, He Y, Cao J, Liu X, Wang M Y, Ma J C, Lai J W, Lu H, Jia S, Yan D Y, Shi Y G, Duan J X, Han J F, Xiao W D, Chen J H, Sun K, Yao Y G, and Sun D 2019 *Nat. Commun.* **10** 5736
[23] Kang K F, Zhao W J, Zeng Y H, Watanabe K, Taniguchi T, Shan J, and Mak K F 2023 *Nat. Nanotechnol.* **18** 861
[24] Sheng H H, Fang Z, and Wang Z J 2023 *Phys. Rev. B* **108** 104109
[25] Deb S, Cao W, Raab N, Watanabe K, Taniguchi T, Goldstein M, Kronik L, Urbakh M, Hod O, and Ben Shalom M 2022 *Nature* **612** 465
[26] Yang Q, Wu M and Li J 2018 *J. Phys. Chem. Lett.* **9** 71604

[27] de la Barrera S C, Cao Q R, Gao Y, Gao Y, Bheemarasetty V S, Yan J Q, Mandrus D G, Zhu W G, Xiao D, and Hunt B M 2021 *Nat. Commun.* **12** 5298

[28] Yang D Y, Wu J D, Zhou B T, Liang J, Ideue T, Siu T, Awan K M, Watanabe K, Taniguchi T, Iwasa Y, Franz M, and Ye Z L 2022 *Nat. Photon.* **16** 469

[29] Wu J, Yang D, Liang J, Werner M, Ostroumov E, Xiao Y, Watanabe K, Taniguchi T, Dadap J I, Jones D, and Ye Z 2022 *Sci. Adv.* **8** 3759

[30] Yasuda K, Wang X R, Watanabe K, Taniguchi T, and Jarillo-Herrero P 2021 *Science* **372** 1458

[31] Yan M Z, Wang E Y, Zhou X, Zhang G Q, Zhang H Y, Zhang K N, Yao W, Lu N P, Yang S Z, Wu S L, Yoshikawa T, Miyamoto K, Okuda T, Wu Y, Yu P, Duan W H, and Zhou S Y 2017 *2D Mater.* **4** 045015

[32] Pi L J, Li L, Liu K L, Zhang Q F, Li H Q, and Zhai T Y 2019 *Adv. Funct Mater.* **29** 1904932

[33] Wang G Z, Wang Z Z, McEvoy N, Fan P, and Blau W J 2021 *Adv. Mater.* **33** 2004070

[34] Henkelman G, Uberuaga B P, and Jónsson H 2000 *J. Chem. Phys.* **113** 9901

[35] Taylor J, Guo H, and Wang J 2001 *Phys. Rev. B* **63** 245407

[36] Blázquez Martínez A, Grysan P, Girod S, Kovacova V, Glinsek S, and Granzow T 2023 *Appl. Phy. Lett.* **122** 152903

[37] Yang M M, Kim D J, and Alexe M 2018 *Science* **360** 904

[38] Xiao R C, Gao Y, Jiang H, Gan W, Zhang C J, and Li H 2022 *npj Comput. Mater.* **8** 138

[39] Lian Y L, Jia S W, Yu H, Han J Y, Jiang J M, Lan C Y, Liu X D, Liao Y L, Dong X, Wang Y, Gou J, Wu Z M, Jiang Y D, and Wang J 2025 *Adv. Mater.* **37** 2404336